Available online at www.sciencedirect.com

ScienceDirect

Procedia Structural Integrity 54 (2024) 536–544

Structural Integrity Procedia

www.elsevier.com/locate/procedia

International Conference on Structural Integrity 2023 (ICSI 2023)

Inflation Mechanics of Aortic Phantoms: An Experimental Study

Hugo Mesquita[1*], Daniela Azevedo[1], Rodrigo Valente[2], Pedro J. Sousa[1], Tiago Domingues[1], Paulo J. Tavares[1], José Xavier[2], Pedro M. G. J. Moreira[1]

[1]INEGI, Rua Dr. Roberto Frias 400, 4200-465 Porto, Portugal
[2]Nova School of Science & Technology, Largo da Torre, 2829-516 Caparica, Portugal

Abstract

A novel approach to understanding aortic mechanics through the study of bulge inflation in silicone aortic phantoms, emphasizing deformation prior to rupture. Recognizing the limitations of current methods that focus on rupture events, our research provides vital empirical data on aortic deformation, a critical aspect in predicting and preventing life-threatening aortic ruptures. By comparing physical experiments with advanced simulation models, we offer a comprehensive analysis that enhances the predictive accuracy of aortic behaviour under stress, contributing significantly to the field of biomedical research and patient safety.

Keywords: Type your keywords here, separated by semicolons ;

1. Introduction

The principal artery of systemic circulation, the aorta, is tasked with channelling oxygenated blood from the left ventricle to the vessels that supply the body. Enduring over 100,000 loading cycles daily, the mechanical integrity of this vessel is critical to human life and a focal point of biomedical research. (Zhu Wenying, 2022) (Wagenseil, 2023) (Sayantan Jana, 2019)

* Corresponding author. Tel.: +351-229-578-710.
E-mail address: hmesquita@inegi.up.pt

2452-3216 © 2023 The Authors. Published by ELSEVIER B.V.

10.1016/j.prostr.2024.01.116

The aorta is a muscular and elastic artery characterized by its hyperelastic and viscoelastic properties. Its resilience is attributed to the abundant presence of vascular smooth muscle and elastin. The intrinsic complexity of these biological tissues poses significant challenges for accurate mechanical property assessment. Factors such as the distribution, arrangement, and proportion of elastin and collagen fibers confer highly nonlinear and anisotropic properties. (Hiromi Yanagisawa, 2020) (Austin J. Cocciolone, 2018)

Standard biaxial tension tests are valuable for analyzing the anisotropic behaviour of aortic tissue. However, they may not entirely replicate the aorta's physiological stress conditions. (Juan A. Peña, 2018) Bulge inflation tests, on the other hand, provide a more comprehensive simulation of the aorta's response under normal physiological conditions. (Mohan, 1983) This approach is particularly beneficial for understanding the aorta's behaviour under typical stress scenarios, offering insights that are more aligned with the regular functioning of the human body.

The aorta's repeated cyclic loading contributes to complex changes in its structure, potentially leading to aneurysms. (Ramella M, 2019) In ascending aortic aneurysms, this process involves concurrent decreases in wall thickness and increases in diameter. Such alterations are frequently accompanied by microstructural changes in elastin or collagen, which can profoundly impact the elasticity and strength of the aorta, culminating in mechanical and functional abnormalities. (Tsamis A, 2013)

The insidious nature of ascending aorta dilation, typically asymptomatic and progressive over the years, underscores the necessity for timely detection. Early identification is crucial to preempt life-threatening events, with surgical intervention often predicated on aneurysmal size. However, the reliance on diameter alone as a parameter for surgical intervention has proven insufficient, as shown by the significant negative correlation between medial wall thickness and aortic diameter in dissection patients, highlighting the need for additional parameters in risk assessment (Van Puyvelde J, 2016).

Understanding the rupture properties of aortic tissues is vital for accurate rupture risk predictions. (Marra, 2006) However, in a clinical setting, the goal is to avoid reaching rupture as it is a critical and life-threatening event. (Quaye, 2022) Therefore, a detailed understanding of the aorta's displacement and material behaviour is critical. The aorta's highly nonlinear and anisotropic properties require sophisticated mathematical models for precise tissue behaviour description (Selmi, 2019; Mourato, et al., 2022).

Using silicone phantom has demonstrated the apparatus's effectiveness in measuring full-field displacements. These results align closely with those calculated by numerical simulations, hinting at the tool's accuracy and reliability. Building on these results, future research will focus on employing this inflation principle using air as a medium to acquire full-field displacements of entire surgically removed human aneurysmatic ascending aortas. A crucial step for advancing our understanding of aortic mechanics in pathological conditions.

Nomenclature

AsAA	Ascending Aorta Aneurysm
DIC	digital image correlation

2. Methods

In an empirical and numerical investigation, the geometric model is critical to the correctness of the results, consequently, it is critical to obtain a truthful geometry of the AsAA. From images obtained using thoracic CT technology a geometric model of an aneurysm patient's ascending aorta was obtained. (Valente, 2021; Valente R, 2022)

a) CT scan images   b) Digital AsAA external shell   c) Silicone phantom

Fig. 1. Silicone phantom development

The obtained external shell was then converted to a solid, considering a thickness of 2mm according to literature. (Choudhury N, 2009) A mold and core were developed with this geometry and the production of the silicone phantom was achieved. The silicone chosen for this phantom was the HB FLEX 5540 as it had very close properties to other silicones documented in the literature, such as the Sylgard™ 184 (Giulia Comunale, 2021), the Prochima® Crystal Rubber (Sina G Yazdi, 2018) or commercially available (Elastrat, 2023) but much simpler potting and curing procedures, as presented in Table 1. From the Silicone phantom, a 25 mm diameter round specimen was cut.

Table 1. Phantom silicone materials' properties (Giulia Comunale, 2021; Sina G Yazdi, 2018; Elastrat, 2023)

Properties	HB Flex 5540	Sylgard™ 184	Prochima® Crystal Rubber	Elastrat
Hardness (Shore A)	40	43	30	40
Cure Time (h)	3	48	24	
Elongation at break (%)	300		350	
Tensile Strenght (MPa)		6.7		6.7
Tear Strength (N/mm)	17.5		3.2	
Specific gravity	1.20	1.03		1.09

2.1. Bulge Test

The bulge test is a method used for the characterization of the soft membrane's mechanical properties. (A.A. Volinsky, 2002) A testing sample cut from the aorta phantom is clamped down between two fixed structures. A pneumatic tube is placed through the bottom part of the fixed rig. As pressurized air is introduced, the specimen deforms outward, forming a spherical surface that protrudes through the circular hole of the top part of the fixed rig. A diagram of the entire setup is presented in Fig. 2. The actuator movement is controlled to maintain a constant testing pressure and through the pneumatic valves, a continuous pressurization is possible allowing for controlled and stable displacement measurements. To obtain full-field displacement measurements three-dimensional digital image correlation (DIC) is used.

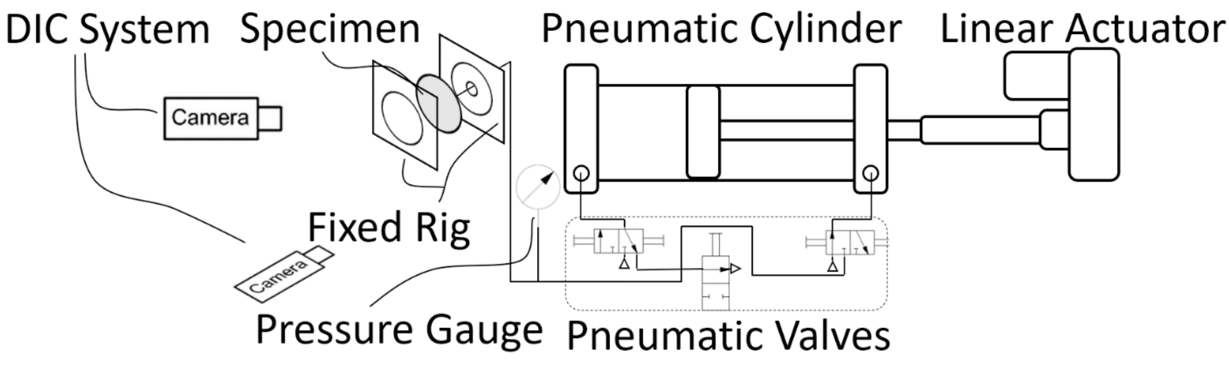

Fig. 2 - Full experimental setup diagram

As the specimen moves and deforms, DIC tracks a mesh of small subsets of the image. To track the pattern in the deformed image, the subsets are adjusted until the pattern in the deformed image matches the reference image as closely as possible; this match is calculated by analyzing the difference in grey levels at each point. The choice of an appropriate speckle pattern plays a vital role in reducing measurement noise and improving the accuracy of the results obtained. (Correlated Solutions, 2021) For this reason, an airbrush with a 0.5mm needle was used to create a detailed

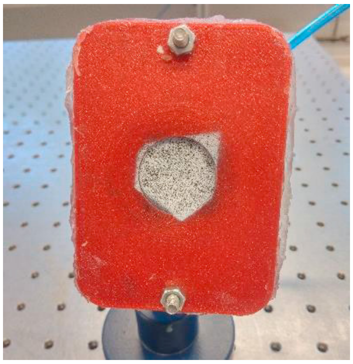

Fig. 3- Clamped Specimen with speckle pattern applied

and refined speckle pattern. As the application of this test was to replicate real biological standards a special water-based ink approved by the hospital histological team was used.

Images were recorded using cameras Gazelle GZL-CL-41C6M-C from Point-Grey, with 16 mm lenses (resolution: 2048 x 2048 pixels). The pressure within the system was gradually increased from a diastolic blood pressure of 80mmHg, and the accompanying displacements were recorded until reaching a systolic pressure of 120 mmHg. A stabilization period was given and only afterwards, the test terminated.

The resulting images were processed using Correlated Solutions Vic 3D. With a subset size of 43 pixels and a subset step of 8 pixels, the displacements were computed.

In Fig. 3- Clamped Specimen with speckle pattern appliedFig. 3 is presented the clamping system with the specimen already painted with the digital image correlation speckle applied.

2.2. Computational Simulation

Given the scarcity of comparable analyses in the literature, computational simulation was employed to compare the obtained results. The aortic structure is characterized as an incompressible, anisotropic material exhibiting hyperelastic nonlinear elasticity. (Ali N. Azadani, 2012) In light of the computational data and since the objective was to validate the bulge measurements, the Neo-Hookean model presented a good compromise between sufficient accuracy, simplicity, and available constants in the literature. (Benjamin Owen, 2018; Parshin, 2019)

The neo-Hookean model is a hyperelastic material model that can be used for predicting the stress-strain behaviour of materials undergoing large deformations. This model also assumes non-linear elastic, isotropic behaviour, and incompressibility, having the strain energy density equation given by Equation 1 (Marwa Selmi, 2019), where μ_s and k represent the shear and bulk modulus, respectively, $\bar{I}_1$ represents the deviatoric part of the first invariant of the stress or strain tensor and J represents the Jacobian determinant of the deformation gradient.

$$U = \frac{\mu_s}{2}(\bar{I}_1 - 3) + \frac{k}{2}(J - 1)^2 \quad (1)$$

The material properties used in this study were derived from a previous investigation that conducted fluid-structure interaction (FSI) simulations to examine the deformation of the cardiac muscle and the behaviour of vessel walls under blood pressure. Table 5.1 presents the properties obtained from this study, which were the ones selected to be used in the present simulation. (Marwa Selmi, 2019)

Table 2. Mechanical parameters of the aorta

Parameter	Unit	Value
Density (ρ)	Kg/m^3	960
Shear Modulus (μ_s)	N/m^2	62.04×10^5
Bulk Modulus (k)	N/m^2	124×10^{-5}

Regarding the Neo-Hooke model in Abaqus, the strain energy function is represented by the Equation 2.

$$U = C_{10}(\bar{I}_1 - 3) + \frac{1}{D_1}(J_{el} - 1)^2 \tag{2}$$

In order to utilize the shear and bulk modulus values in the context of the Abaqus software, a conversion process was undertaken to obtain the corresponding C10 and D1 constants. These values are depicted in Table 3, which specifically shows the values employed in Abaqus density and hyperelasticity parameters.

Table 3. Values used in the simulation for the Neo-Hooke model

Parameter	Unit	Value
ρ	g/mm^3	960
C_{10}	N/mm^2	3.102
D_1	mm^2/N	0.16129

The geometry used in the simulation was based on the external area of the silicone specimen, resulting in a circular shape with a diameter of 25 mm and a thickness of 2 mm.

A load was defined for each step to replicate the corresponding pressure levels. In the first step, a pressure of 0.107 MPa (80 mmHg) was applied to simulate the diastolic blood pressure, while in the second step, a pressure of 0.16 MPa (120 mmHg) was implemented to emulate the systolic blood pressure. The pressure load was specifically applied to one side of the specimen to represent the region within the mechanism where the pneumatic tube exerts pressure. This pressure is distributed across the specimen's circular groove.

A pinned boundary condition was implemented across the thickness of the sample region to restrict any movement of the silicone specimen within the mechanism. This boundary condition attempts to reflect the fixation of the specimen inside the mechanism. The meshing process in the simulation utilized 21236 C3D10 elements.

To ensure consistency between computational and experimental procedures, post-processing was applied after simulations. A new coordinate system was established using a midpoint reference from the specimen tips. This alignment aimed to replicate the experimental setup closely. Afterwards, displacement differences were measured under two pressures: diastolic (80 mmHg) and systolic (120 mmHg). The resulting displacement data will be discussed in subsequent sections.

3. Results and Discussion

The graph presented in Fig. 4 shows the measured pressure values during the bulge test. It is possible to observe minor fluctuations in pressure and a rapid transition between diastolic (80 mmHg) and systolic (120 mmHg) pressure. However, there is a decrease in the measured pressure at the diastolic plateau, attributable to minor leakages and insufficient correction from the controlled linear actuator movement. Nonetheless, these changes never exceeded 2.5% of the defined value.

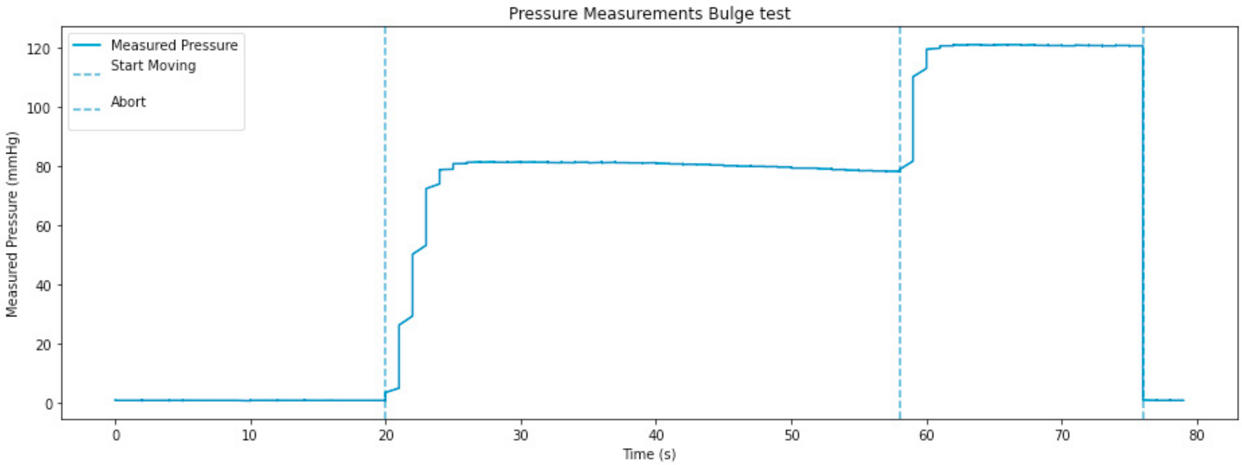

Fig. 4- Measured and defined pressured bulge test

Fig. 5 presents the displacement results in the X direction obtained from the experimental part and from the computational simulation, respectively.

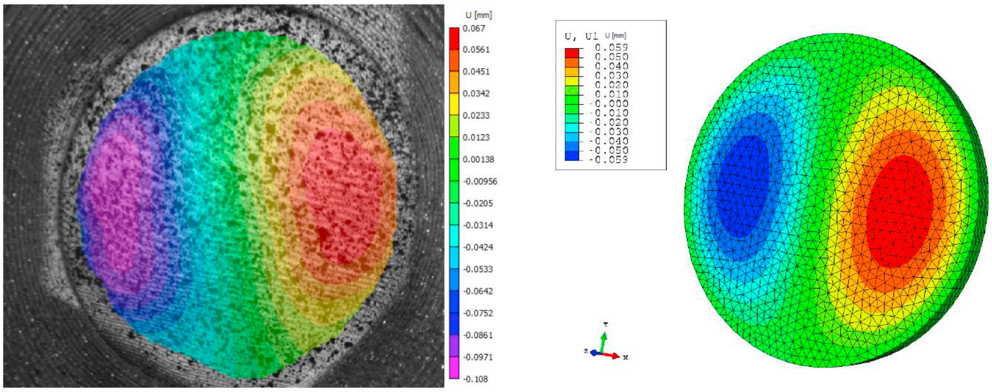

a) Experimental results in the X direction *b) Simulations results in the X direction*

Fig. 5. Comparison of the displacement in the X direction between experimental and computational

In the study, both experimental and computational methods showed similar displacement patterns, indicating consistency in the results. The experimental data presented a near-symmetrical distribution of displacement values on both sides, though with some differences. Specifically, the maximum displacement on the left side was 0.067 mm, and on the negative side, on the left, it was 0.108 mm. The computer simulation, on the other hand, exhibited a maximum displacement of 0.059 mm, symmetric on both sides. The experimental discrepancy could be due to different pre-stresses caused by the specimen placement on the rig or manufacturing errors on the silicone phantom.

Results in the Y direction are similar although with better approximation between the negative and opposite sides in the experimental measurements. The positive displacement was 0.101 mm and the negative 0.093 mm. As the X direction has more meaningful results the Y direction was not presented in this work.

A notable distinction was observed in the region of zero or nearly zero displacement. In the computer simulation, this occurred not only in the central area but also at the tips, whereas in the experimental setup, it was limited to the central area, with the tips showing increased displacement. This difference could be due to the material not being completely embedded in the experimental setup, allowing more movement at the corners. Despite these variances, both methods displayed largely congruent behaviour overall. While specific specimen regions variations existed, the general trends and patterns of displacement were similar, suggesting that both approaches effectively captured the fundamental behaviour and response of the system.

Regarding the values in the Z direction presented in Fig. 6, both the experimental and simulation analyses demonstrate the presence of a distinct central zone with higher displacements. In the experimental analysis, the maximum displacement magnitude registered is 0.658 mm, while in the simulation, it reaches 0.501 mm. This indicates significant deformation in the central area in both cases.

However, there are some disparities between the two methods. In the experimental analysis, the displacement gradually decreases as we move away from the central zone towards the tips, with a minimum value of 0.218 mm. In contrast, the simulation results show a reduction in displacement towards the corners, eventually reaching zero. The displacement behaviour in the corners may be influenced by three factors, as said previously: the fixed boundary condition in the simulation, which restricts displacement towards the corners; the material's relative freedom of movement in the experimental part, which can cause variations; and the limited coverage of the analyzed area by DIC, excluding the edges.

Overall, while the magnitudes of displacement differ slightly between the experimental and simulation results, the overall trends align with the expected mechanical response of the silicone sample during the bulge inflation test. These findings suggest that both methods capture the fundamental behaviour of the sample during the inflation process, albeit with some nuanced variations. In conclusion, the experimental testing conducted with the silicone sample can be considered to closely approximate the simulation results obtained using the properties of aortic tissue.

The neo-Hookean model predicts non-linear behaviour for elastic, isotropic, incompressible material at increasing strains. Allowing to have good results when comparing to experimental silicone deformations. The findings on aorta properties do, however, show different behaviour at higher stresses, which is caused by the change in the orientation of collagen fibers in the vessel wall (Benjamin Owen, 2018). Several hyperelastic models, including exponential models and models that integrate fiber orientation, have been presented that could be applied to these study. Before selecting and adopting such a model, a detailed comparison of different models is required, as is an assessment of their identifiability. This, however, is outside the scope of the current investigation mostly because of the large number of parameters and the input required, many of these models are not applicable in vivo.

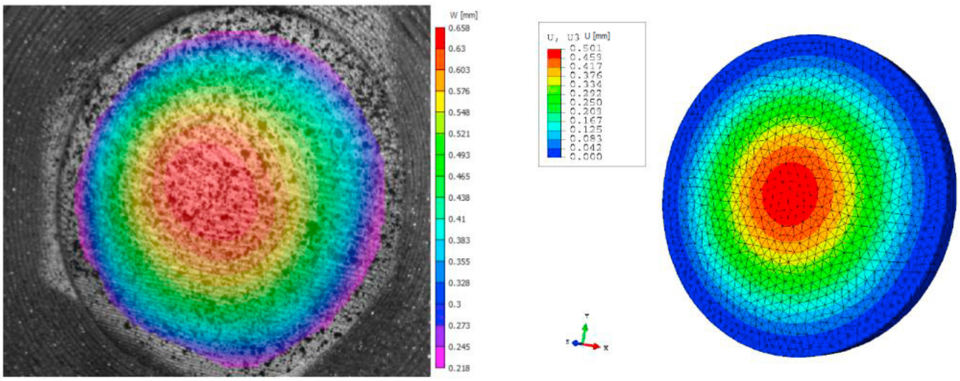

a) *Experimental results in the Z direction* *b) Simulations results in the Z direction*

Fig. 6. Comparison of the displacement in the Z direction between experimental and computational

4. Conclusions and future work

The experimental approach, incorporating the bulge inflation test complemented by digital image correlation, has proven effective in providing insights into its biomechanical properties.

The empirical results have been particularly enlightening in demonstrating the silicone phantom's ability to mimic the mechanical behaviour of the aorta. These findings, closely aligned with the predictions of the computational Neo-Hookean model, highlight the potential of using silicone models in biomechanical studies. While the silicone phantom cannot replicate all the complexities of biological aortic tissue, its behaviour under stress provides a useful approximation for understanding the fundamental mechanical properties of the aorta, especially in terms of displacement under varying pressure conditions. Besides allowing for a validation of the experimental setup and the use of air as a pressure fluid.

Our research underscores the importance of accurate biomechanical modelling in understanding vascular health. By bridging the gap between theoretical models and practical, clinical applications, we can better predict, diagnose, and treat aortic diseases, ultimately contributing to improved patient outcomes and healthcare.

In the future, this setup will work to pressurize and measure the differences in displacements between systolic and diastolic pressure from an entire surgically removed AsAA. Therefore, having this proof of concept allows for a more secure and stable development of the next steps.

Acknowledgements

This work was developed in the scope of the project AneurysmTool - Refª PTDC/EMD-EMD/1230/2021, funded by "FCT Projetos I&D" of the "Fundação para a Ciência e a Tecnologia"

References

A.A. Volinsky, N. M. (2002). Interfacial toughness measurements for thin films on substrates. *Acta Materialia*.

Ali N. Azadani, S. C. (2012). Comparison of Mechanical Properties of Human Ascending Aorta and Aortic Sinuses. *The Annals of Thoracic Surgery*.

Austin J. Cocciolone, J. Z. (2018). Elastin, arterial mechanics, and cardiovascular disease. *American Journal of Physiology-Heart and Circulatory Physiology*.

Benjamin Owen, N. B. (2018). Structural modelling of the cardiovascular system. *Biomechanics and Modeling in Mechanobiology*.

Choudhury N, B. O. (2009). Local mechanical and structural properties of healthy and diseased human ascending aorta tissue. *Cardiovascular pathology : the official journal of the Society for Cardiovascular Pathology*.

Correlated Solutions. (2021). *Speckle Pattern Fundamentals.*

Elastrat. (2023, 9 20). *Anatomical vascular models*. Retrieved from https://www.elastrat.com/

Giulia Comunale, L. D. (2021). Numerical models can assist choice of an aortic phantom for in vitro testing. *Bioengineering*.

Hiromi Yanagisawa, J. W. (2020). Elastic fibers and biomechanics of the aorta: Insights from mouse studies. *Matrix Biology*.

Juan A. Peña, V. C. (2018). Over length quantification of the multiaxial mechanical properties of the ascending, descending and abdominal aorta using Digital Image Correlation. *Journal of the Mechanical Behavior of Biomedical Materials*.

Marra, S. K. (2006). Elastic and Rupture Properties of Porcine Aortic Tissue. *Cardiovasc Eng* .

Marwa Selmi, H. B. (2019). Numerical Study of the Blood Flow in a Deformable Human Aorta. *Applied Sciences*.

Mohan, D. M. (1983). Failure properties of passive human aortic tissue. II--Biaxial tension tests. *Journal of Biomechanics*.

Mourato, A., Valente, R., Xavier, J., Brito, M., Avril, S., de Sá, J., . . . Fragata, J. (2022). Computational Modelling and Simulation of Fluid Structure Interaction in Aortic Aneurysms: A Systematic Review and Discussion of the Clinical Potential. *Applied Sciences*.

Parshin, D. L. (2019). On the optimal choice of a hyperelastic model of ruptured and unruptured cerebral aneurysm.

Scientific Reports.
Quaye, K. B.-B. (2022). Contemporary Management of Abdominal Aortic Aneurysms. *Current cardiology reports*.
Ramella M, B. G. (2019). Effect of Cyclic Stretch on Vascular Endothelial Cells and Abdominal Aortic Aneurysm (AAA): Role in the Inflammatory Response. *Int J Mol Sci*.
Sayantan Jana, M. H. (2019). Extracellular matrix, regional heterogeneity of the aorta, and aortic aneurysm. *Exp Mol Med*.
Selmi, M. H. (2019). Numerical Study of the Blood Flow in a Deformable Human Aorta. *Applied Sciences*.
Sina G Yazdi, P. G. (2018). A review of arterial phantom fabrication methods for flow measurement using piv techniques. *Annals of Biomedical Engineering*.
Tsamis A, K. J. (2013). Elastin and collagen fibre microstructure of the human aorta in ageing and disease: a review. *J R Soc Interface*.
Valente R, M. A. (2022). Fluid–Structure Interaction Modeling of Ascending Thoracic Aortic Aneurysms in SimVascular. *Biomechanics*.
Valente, R. (2021). Estudo numérico da interaçãao fluido-estrutura numa aorta ascendente. *Master's thesis, Universidade NOVA de Lisboa, Lisboa, Portugal*.
Van Puyvelde J, V. E. (2016). Aortic wall thickness in patients with ascending aortic aneurysm versus acute aortic dissection. *Eur J Cardiothorac Surg*.
Wagenseil, J. E. (2023). The matrix reloaded - Addressing structural integrity of the aortic wall in aneurysmal disease. *Biomater Biosyst*.
Zhu Wenying, W. Y. (2022). Dynamic Changes in the Aorta During the Cardiac Cycle Analyzed by ECG-Gated Computed Tomography. *Frontiers in Cardiovascular Medicine*.